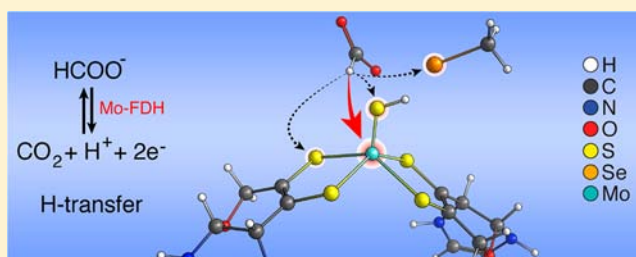


Evidence for the Formation of a Mo–H Intermediate in the Catalytic Cycle of Formate Dehydrogenase

Matteo Tiberti,[†] Elena Papaleo,[†] Nino Russo,[‡] Luca De Gioia,[†] and Giuseppe Zampella^{*,†}[†]Department of Biotechnology and Biosciences, University of Milano-Bicocca, Piazza della Scienza 2, 20126 Milan, Italy[‡]Department of Chemistry, University of Calabria, via P. Bucci, Arcavacata di Rende (CS) 87036, Italy

S Supporting Information

ABSTRACT: DFT/BP86/TZVP and DFT/B3LYP/TZVP have been used to investigate systematically the reaction pathways associated with the H-transfer step, which is the rate-determining step of the reaction $\text{HCOO}^- \rightleftharpoons \text{CO}_2 + \text{H}^+ + 2\text{e}^-$, as catalyzed by metalloenzyme formate dehydrogenase (FDH). Actually, the energetics associated with the transfer from formate to all H (proton or hydride) acceptors that are present within the FDH active site have been sampled. This study points to a viable intimate mechanism in which the metal center mediates H transfer from formate to the final acceptor, i.e. a selenocysteine residue. The Mo-based reaction pathway, consisting of a β -H elimination to metal with concerted decarboxylation, turned out to be favored over previously proposed routes in which proton transfer occurs directly from HCOO^- to selenocysteine. The proposed reaction pathway is reminiscent of the key step of metal-based catalysis of the water–gas shift reaction.



INTRODUCTION

Accumulation of carbon dioxide (CO_2) in the atmosphere is nowadays recognized as the main contributor to the greenhouse effect and anthropogenic global warming. That is why the catalytic conversion of CO_2 to liquid fuels and synthetic organic and inorganic chemicals has become of primary interest. CO_2 transformation into value-added commodities is, however, a very challenging task because of CO_2 thermodynamic stability and kinetic inertness. Nonetheless, CO_2 is an inexpensive, abundant, and nontoxic C_1 feedstock, to the extent that its photo- and electroreduction to CH_3OH , HCOOH , and CH_4 (among many others) and their use as carbon-neutral energy carriers has been deserving ever-increasing consideration.^{1–3} Among all possible half-cell reactions for the electroreduction of CO_2 , the $\text{CO}_2 + \text{H}^+ + 2\text{e}^- \rightleftharpoons \text{HCOO}^-$ reaction displays the best chance for practical developments.⁴ Moreover, formic acid is a potential high-value fuel for fuel-cell applications. In addition, among C_1 chemicals, formic acid is suggested to provide the highest monetary value for the energy required to form it.⁵ Formate possesses an oxidation potential similar to that of hydrogen and, therefore, could also be used to conveniently transport and store the reduction potential of dihydrogen⁶ or used in a cycle of direct electrochemical oxidation/reduction to/from CO_2 .

The direct interconversion $\text{CO}_2 + \text{H}^+ + 2\text{e}^- \rightleftharpoons \text{HCOO}^-$ is catalyzed by the metalloenzyme formate dehydrogenase (FDH). In fact, the enzymatic electrode-coupled reduction of CO_2 , turned over by FDH, has been reported to be characterized by high efficiency and specificity,⁷ features that are appealing for industrial applications. In enterobacteria, such

as *Escherichia coli*, FDHs are part of higher-level complexes and efficiently oxidize HCO_2^- to CO_2 ; the electrons thus obtained are conducted to other catalytic centers, where a substrate is reduced.⁸

The active site of bacterial FDHs (Figure 1, left) hosts a transition-metal coordination compound, formed by two molybdopterin guanine dinucleotide (MGD) cofactors coordinating a single Mo or, more rarely, a W atom.⁹ The MGDs are formed by a dithiolene–pyranopterin moiety (molybdopterin or MPT) bound to an alkyl diphosphate guanine nucleotide. Metal coordination takes place via bis-chelation of the S atoms of dithiolene. This bis(MGD)Mo complex is typical of the dimethyl sulfoxide (DMSO) reductase protein family, whose members catalyze redox reactions usually involving oxygen transfer.¹⁰ In the FDHs, the coordination sphere of Mo^{VI} is completed by the selenide of a deprotonated selenocysteine (Se-Cys) residue and a sulfur ligand (SH^- or S^{2-}). FDHs usually also host other metal centers, such as Fe_xS_y clusters, used for electron transport.

The reaction mechanism underlying the catalytic oxidation of formate by FDH has not been completely elucidated yet, although some proposals, deriving from both experimental and computational studies, have been reported.^{11–14} Unlike other members of the DMSO reductase family, the FDH catalytic reaction involves direct proton transfer,¹⁵ which is the rate-determining step of the whole catalytic process.¹¹ Previously proposed mechanisms for formate oxidation start with the

Received: April 27, 2012

Published: July 16, 2012

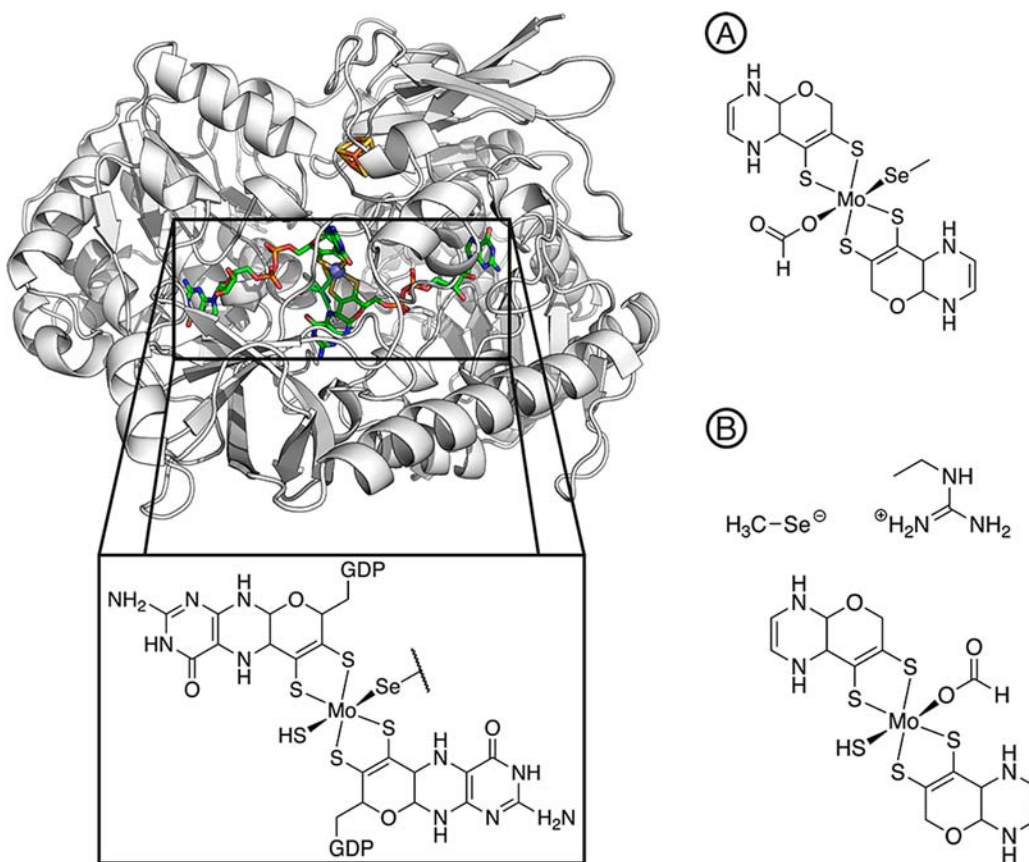


Figure 1. Left: *E. coli* FDH-H with highlighted bis(MGD)Mo^{IV}, in sticks. Right: Models A and B used in this study, displaying all of the atoms treated at the DFT level.

replacement of one of the Mo^{VI} ligands by a substrate, with subsequent proton abstraction and electron transfer to the metal ion, which is thus reduced to Mo^{IV}. Two models of the reaction mechanism have been suggested for the proton-transfer step, both involving the same proton acceptor: in the first (usually denoted as A), formate displaces the sulfur ligand (SH⁻ or S²⁻) and proton abstraction is performed by the Se atom of Se-Cys, which remains coordinated to the Mo ion;¹⁴ in the second (B), formate replaces the selenium ligand in the metal coordination environment, and proton abstraction is performed by the unbound selenide.¹² Such two reaction pathways have been previously investigated by density functional theory (DFT), with mechanism B as both thermodynamically and kinetically favored.¹³ A more recent work¹¹ on the modeling of the full catalytic cycle also proposed that the proton abstraction step is performed by the unbound Se-Cys.

Even though the basic properties of Se-Cys and its location within the active site are consistent with the proposed role of the proton acceptor in the FDH catalytic cycle, nevertheless, other atoms coordinating the Mo^{VI} ion can act as putative proton acceptors: (i) the S atoms belonging to the dithiolene moiety of the MGD cofactor, (ii) the SH⁻ (or S²⁻) group, and (iii) the Mo ion itself, through a hydride-transfer step. Therefore, with the aim of shedding further light on one of the key steps in the reaction catalyzed by FDH, we have investigated by DFT all of the possible pathways of H⁺ or H⁻ transfer from formate to the enzyme active site.

COMPUTATIONAL METHODS

All of the performed DFT calculations have been carried out using a valence triple- ζ basis set with polarization on all atoms (TZVP)¹⁶ and the pure exchange-correlation functional BP86.^{17,18} The inner-core 28 electrons of the Mo ion have been treated using a relativistic effective-core potential (ecp-28-mwb; $\lambda_{\max} = 3$),¹⁹ whereas the valence electronic structure has been investigated by the same full-electron basis (TZVP) that has been employed for the rest of the system. The chosen computational setup permitted to accurately reproduce the distances between the Mo^{VI} ion and the S and Se atoms of the first coordination sphere, as found in the *E. coli* FDH-H crystal structure (PDB ID 1FDO;¹⁴ see Table 1). Moreover, the BP86 functional has been shown to appropriately describe chemical systems involving CO₂-metal interactions.^{20,21}

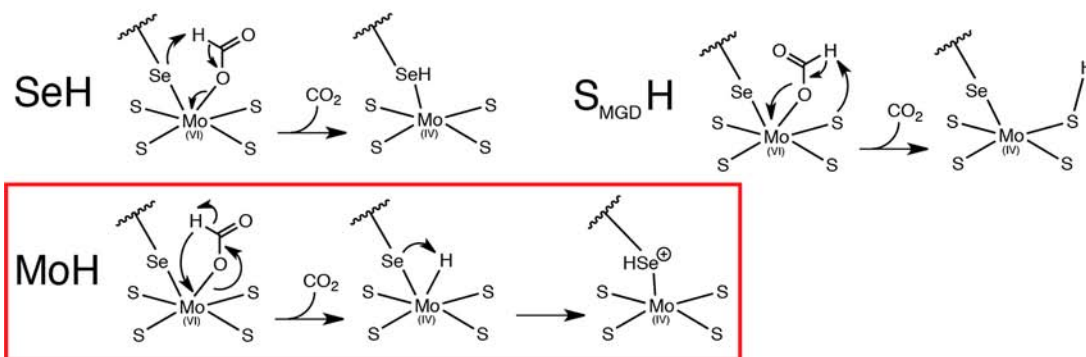
The reported calculations have been performed by employing a protein-like dielectric constant value ($\epsilon = 4$) as implemented in the COSMO²² solvation model. Anyway, it has been verified that moderate changes (less than 2 kcal mol⁻¹) can be detected by

Table 1. Experimental versus Computed Comparison Regarding Interatomic Distances between the Mo Ion and the S or Se Atoms Identified in the First Coordination Sphere

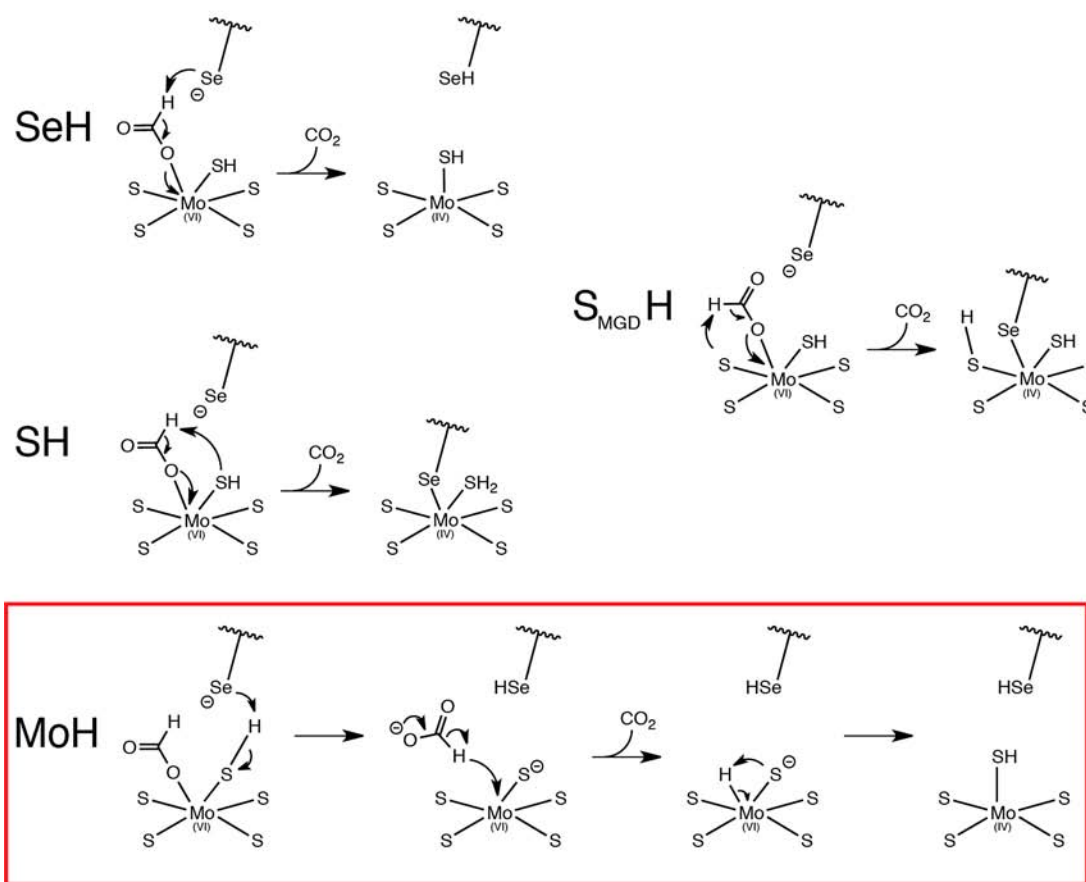
	X-ray (1FDO; Å)	calculations (BP86/TZVP; reactant state; Å)
Mo-S _{MGD1}	2.35	2.39
Mo-S _{MGD2}	2.49	2.41
Mo-S _{MGD3}	2.44	2.41
Mo-S _{MGD4}	2.37	2.39
Mo-Se	2.60	2.54

Scheme 1. Investigated Reaction Mechanisms of H Transfer Related to FDH Catalysis^a

Model A



Model B



^aThe only transfer occurring as a hydride (via a metal center) is boxed in red.

switching from energetics computed in vacuo and by including an implicit solvation model. DFT calculations have been carried out using the TURBOMOLE suite of programs.²³

Stationary points of the energy hypersurface have been located by means of energy-gradient techniques. Geometry optimization has been carried out on starting structure guesses. Starting atomic positions were derived, for both models A and B, from the *E. coli* FDH-H crystal structure (PDB ID 1FDO), in which the Mo atom was in the oxidized state of Mo^{VI}. For model A, the SH ligand was replaced by a formate molecule. For model B, the CH₃Se⁻ moiety was moved away from the Mo coordination sphere, interacting with the arginine (Arg) moiety. A

formate molecule was placed instead in the Mo coordination sphere. Amino acid models employed in the present study were permitted to move freely during the optimizations, in order to avoid obtaining artificial negative eigenvalues in the Hessian matrix evaluation. Indeed, the actual shift of such residues that we used for B-type mechanisms has been observed to be quite limited in extent, and especially it has been found to be compatible with the overall structure of the enzyme active-site region, as observed in the crystal structures. Moreover, it is noteworthy that the region that hosts the active site can be highly dynamical: for instance, the Se-Cys residue has been found to be able to move drastically (up to more than 12 Å) with respect to its position

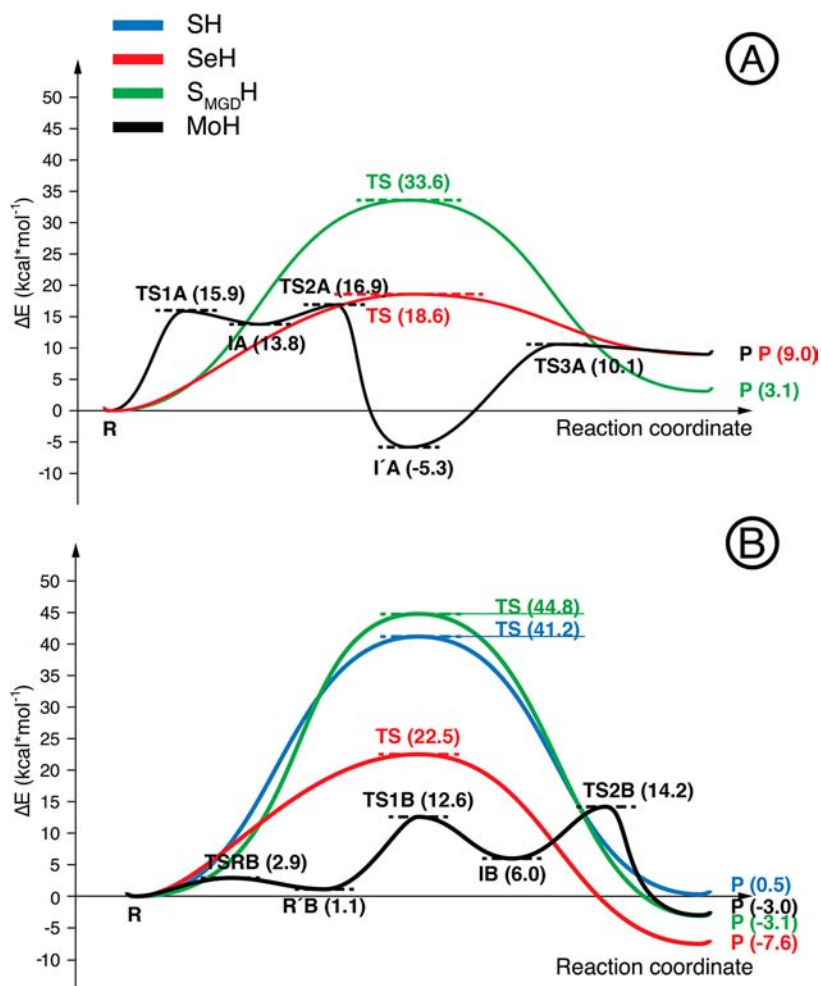


Figure 2. Reaction profiles associated with all investigated pathways of proton transfer at the DFT/BP86 level.

in the Mo-bound form.¹² We thus deemed that fixing residues or tightly constraining them in their initial positions would have limited their conformational freedom in an unrealistic fashion.

The optimization of transition-state structures has been carried out according to a procedure based on a pseudo-Newton–Raphson method. Initially, geometry optimization of a transition-state guess geometry is performed, keeping the distances corresponding to the selected reaction coordinate constrained. Normal-mode analysis at the BP86/TZVP level is then carried out on the constrained minimum-energy structures, and if one imaginary vibrational frequency corresponding to the reaction coordinate is found, the curvature determined at such a point is used as the starting point for the next phase. Finally, the transition-state search is performed according to an eigenvector-following search procedure, in which the eigenvectors in the Hessian are sorted in ascending order, with the first one being that associated with a negative eigenvalue. After the first step, however, the search is performed by choosing the critical eigenvector with a maximum overlap criterion, which is based on the dot product with the eigenvector followed at the previous step.

NBO/NPA²⁴ partition schemes of the electron density have been used for determining the atomic partial charges. All of the ΔE values discussed in the present contribution have been calculated as differences between pure electronic energies. A B3LYP²⁵ exchange-correlation functional has finally been used to check the consistency of the BP86 results (related energy profiles are reported in the Supporting Information)

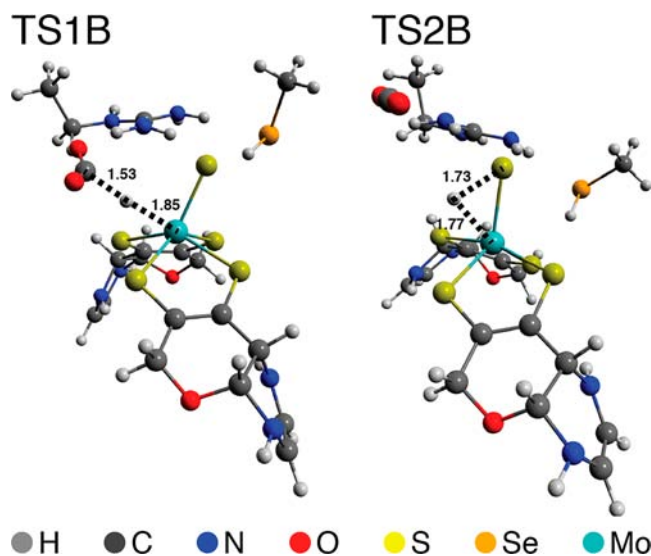


Figure 3. Relevant transition states of the mechanism MoH-B. Structural elements forming the reaction coordinate are in angstroms.

RESULTS AND DISCUSSION

Once verified that the adopted computational setup can reproduce accurately the structural features of the Mo cofactor (see the Computational Methods section; Table 1), we have

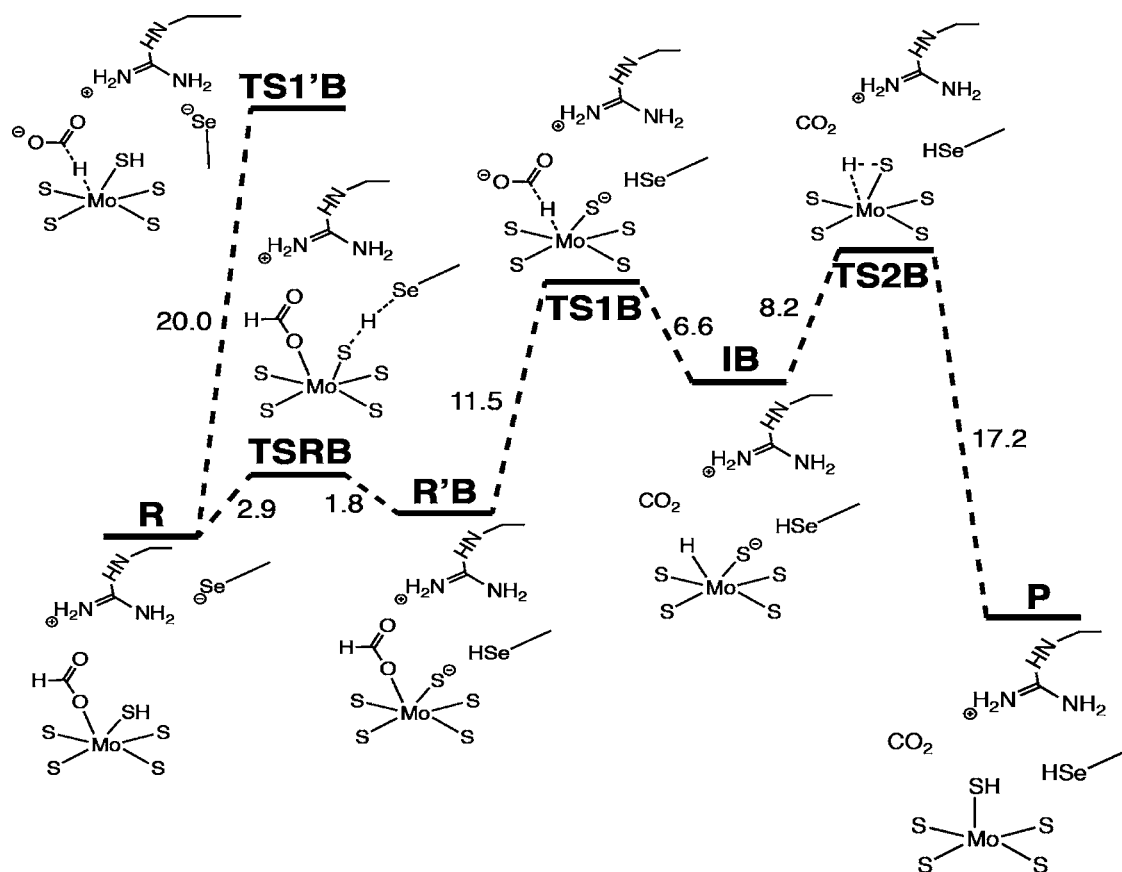


Figure 4. Energy profile (kcal mol^{-1}) of the MoH-B reaction pathway.

Table 2. Calculated Partial Charges (NBO) Associated with MA Stationary Points^a

	R	SeH TS	SeH P	$S_{\text{MGD}}\text{H TS}$	$S_{\text{MGD}}\text{H P}$	MoH TS1A	MoH IA	MoH TS2A	MoH I'A	MoH TS3A
$O_{1\text{formate}}$	-0.60	-0.50	-0.48	-0.51	-0.45	-0.54	-0.53	-0.48	-0.46	-0.46
$O_{2\text{formate}}$	-0.50	-0.43	-0.40	-0.42	-0.47	-0.51	-0.50	-0.45	-0.46	-0.46
H_{formate}	0.10	0.00	0.08	0.03	0.18	0.06	0.11	0.03	0.06	0.13
Mo	0.04	-0.19	-0.29	-0.19	-0.27	-0.23	-0.23	-0.35	-0.35	-0.31
Se	0.24	0.43	0.34	0.18	0.17	0.19	0.21	0.18	0.31	0.32
S2	0.16	0.14	0.17	0.16	0.10	0.27	0.29	0.27	0.14	0.18
S3	0.17	0.14	0.16	0.26	0.20	0.15	0.17	0.26	0.13	0.15
S4	0.24	0.18	0.14	0.13	0.13	0.14	0.21	0.20	0.21	0.13
S1	0.19	0.19	0.12	0.30	0.24	0.24	0.27	0.25	0.16	0.14
C2	-0.21	-0.23	-0.23	-0.16	-0.16	-0.23	-0.23	-0.23	-0.22	-0.21
C3	-0.21	-0.20	-0.21	-0.23	-0.20	-0.23	-0.19	-0.21	-0.18	-0.20
C4	-0.23	-0.21	-0.21	-0.21	-0.21	-0.21	-0.24	-0.23	-0.24	-0.21
C1	-0.23	-0.20	-0.19	-0.25	-0.22	-0.23	-0.21	-0.21	-0.20	-0.20

^aAtoms named S_n are those coordinating the Mo atom in the cofactor model; the corresponding C_n atoms are the C cofactor atoms binding the respective S atoms.

studied the proton-transfer step using the two models of the active site that were adopted in precedent DFT studies: in the first, HCOO^- replaces the SH^- group in the Mo coordination sphere (A; Figure 1, top right); in the second, HCOO^- displaces the Se ligand (B; Figure 1, bottom right).

In the following, the two different cofactor configurations will be referred to as mechanism-model A (denoted as MA) and mechanism-model B (denoted as MB). In both cases, the enzyme active site has been modeled including the Mo center and some of the surrounding residues, which are found in the *E. coli* FDH-H. Previous DFT studies^{11,13} of such systems used two simple dimethyldithiolene moieties to model the MGD

cofactors; however, a very recent investigation pointed out that the organic portion of the cofactor (and its synthetic analogues) is *non-innocent* with respect to redox reactions and that a more extended model should be used to better represent the chemical properties of the MPT.²⁶ Therefore, the two MGD groups have been represented as dithiolene-pyranopyrazine, which has been reported to be the optimal candidate in terms of the accuracy/computational cost ratio.^{26a} The inorganic S ligand coordinated to Mo was modeled initially as SH^- ,¹³ and the Se-Cys residue was modeled by CH_3Se^- (or by the full residue, *vide infra*). Because the MB model features a more negative overall charge with respect to MA, due to the presence

Table 3. Calculated Partial Charges (NBO) Associated with MB Stationary Points^a

	R	SeH R	SeH TS	SeH P	S _{MGD} H TS	S _{MGD} H P	SH TS	SH P
C	0.59	0.58	0.74	0.93	0.65	0.94	0.6	0.93
O1 _{formate}	-0.59	-0.60	-0.56	-0.45	-0.58	-0.42	-0.59	-0.45
O2 _{formate}	-0.64	-0.61	-0.53	-0.48	-0.58	-0.51	-0.63	-0.48
H _{formate}	0.10	0.10	0.04	0.12	0.06	0.14	0.11	0.16
Mo	0.10	0.11	0.01	0.10	0.05	-0.20	-0.09	-0.23
Se	-0.29	-0.28	-0.05	0.00	-0.28	-0.03	-0.30	-0.16
S2	0.14	0.16	0.13	0.10	0.13	0.12	0.16	0.10
S3	0.10	0.16	0.04	0.02	0.23	0.24	0.13	0.04
S4	0.14	0.12	0.20	0.07	0.10	0.05	0.15	0.09
S1	0.18	0.15	0.18	-0.10	0.09	0.11	0.11	0.00
C2	-0.22	-0.23	-0.20	-0.22	-0.22	-0.22	-0.22	-0.25
C3	-0.22	-0.25	-0.21	-0.19	-0.25	-0.24	-0.23	-0.20
C4	-0.24	-0.22	-0.20	-0.22	-0.18	-0.17	-0.24	-0.23
C1	-0.25	-0.23	-0.23	-0.19	-0.22	-0.23	-0.23	-0.24
S5	-0.26	-0.31	-0.38	-0.45	-0.25	-0.46	-0.06	-0.04
H(S5)	0.15	0.16	0.13	0.15	0.00	0.15	0.16	0.17
	MoH TSRB	MoH R'	MoH TS1B	MoH IB	MoH TS2B	MoH P	[HMo(CO) ₅] ⁻	
C	0.59	0.58	0.82	0.93	0.93	0.93	-	-
O1 _{formate}	-0.59	-0.59	-0.61	-0.45	-0.45	-0.45	-	-
O2 _{formate}	-0.63	-0.65	-0.48	-0.49	-0.45	-0.47	-	-
H _{formate}	0.08	0.08	-0.03	0.02	0.14	0.12	-	-
Mo	-0.01	0.01	-0.25	-0.29	-0.20	0.12	-1.00	-
Se	-0.07	-0.03	-0.04	-0.03	-0.03	-0.02	-	-
S2	0.17	0.17	0.17	0.11	0.06	-0.11	-	-
S3	0.20	0.20	0.10	0.09	0.09	0.03	-	-
S4	0.14	0.15	0.13	0.13	0.13	0.02	-	-
S1	0.11	0.11	0.16	0.11	-0.01	0.13	-	-
C2	-0.24	-0.23	-0.22	-0.24	-0.25	-0.20	-	-
C3	-0.24	-0.24	-0.23	-0.23	-0.23	-0.20	-	-

^aAtoms named *Sn* are those coordinating the Mo atom in the cofactor model; the corresponding *Cn* atoms are the C cofactor atoms binding the respective S atoms.

of both CH₃Se⁻ and SH⁻, to offset the negative charge, a protonated dimethylguanidine group was added to mimic Arg333, which is found in the active site of FDH.

The following proton/hydride acceptors were tested for H⁻(CO₂)⁻ transfer in both models A and B (see Scheme 1 for formal reaction schemes): i) the Mo-bound Se atom (referred to as SeH-A mechanism in the following) and the Mo-unbound Se (SeH-B mechanism); ii) one of the MGD thioleues (S_{MGD}H-A and -B mechanisms; with Se-Cys either bound or unbound to Mo, respectively); iii) the Mo(VI) ion, through hydride transfer (MoH-A and -B mechanisms; with Se-Cys either bound or unbound to Mo, respectively). In pathway iii) also the subsequent H⁺ transfer step from the metal hydride to the Se or S atoms found in the active site has been investigated.

Concerning MB, the case in which the SH⁻ ligand performs H⁺ abstraction has also been considered, which is not possible in MA (where SH⁻ is absent because it is replaced by HCO₂⁻). In addition, previous studies illustrating only SeH pathways pointed out that the presence of a conserved histidine (His) residue substantially lowers the energy barrier for proton transfer to the unbound selenide. To take this effect into account, the SeH-B reaction pathway has been studied using a modified MB in which the entire His-Se-Cys dipeptide (the two residues are consecutive in the amino acidic sequence of FDH-H) was included. The reaction pathways have been investigated adopting the *S* = 0 spin state for MA and the *S* = 1 spin state for MB. Such different spin multiplicity characterizing MA and MB

has been recently determined by Russo and co-workers, in the case of Se-based H⁺-transfer pathways.¹³

All computed reaction energy profiles are shown in Figure 2.

The proton-transfer reaction involving S or Se as a final acceptor occurs as an elementary reaction event, whereas the MoH-A and -B pathways are characterized by the formation of an intermediate species. In both MA and MB, H⁺ transfer to the MGD thioleues always features high energy barriers (33.6 kcal mol⁻¹ for MA; 44.8 kcal mol⁻¹ for MB), and this holds true also for transfer to the SH ligand in MB (41.2 kcal mol⁻¹). MoH-A and SeH-A pathways are characterized by energy barriers that slightly favor the former (15.9 and 18.6 kcal mol⁻¹, respectively), while in the SeH-B pathway, the energy barrier is significantly higher than that in MoH-B (22.5 and 11.5 kcal mol⁻¹, respectively).

As for thermodynamics, all MA pathways are endergonic, whereas among MB pathways, the SeH, S_{MGD}H, and MoH routes feature exergonic profiles.

Structural analysis of the stationary points located using DFT shows that H⁺ transfer to either Se or S involves a simple H⁺ shift from formate to the acceptor atom. In the reactants (in both MA and MB), the metal center has a trigonal-prismatic coordination geometry, with one HCO₂⁻ O atom and a Se or S atom (depending on the model) to complete the coordination environment of Mo. In MA, the Se ligand is coordinated to the Mo ion, whereas in MB, it interacts with Arg (2.43 Å). Such an interaction is consistent with the crystal structure of reduced *E. coli* FDH-H, in which the uncoordinated Se-Cys was found to

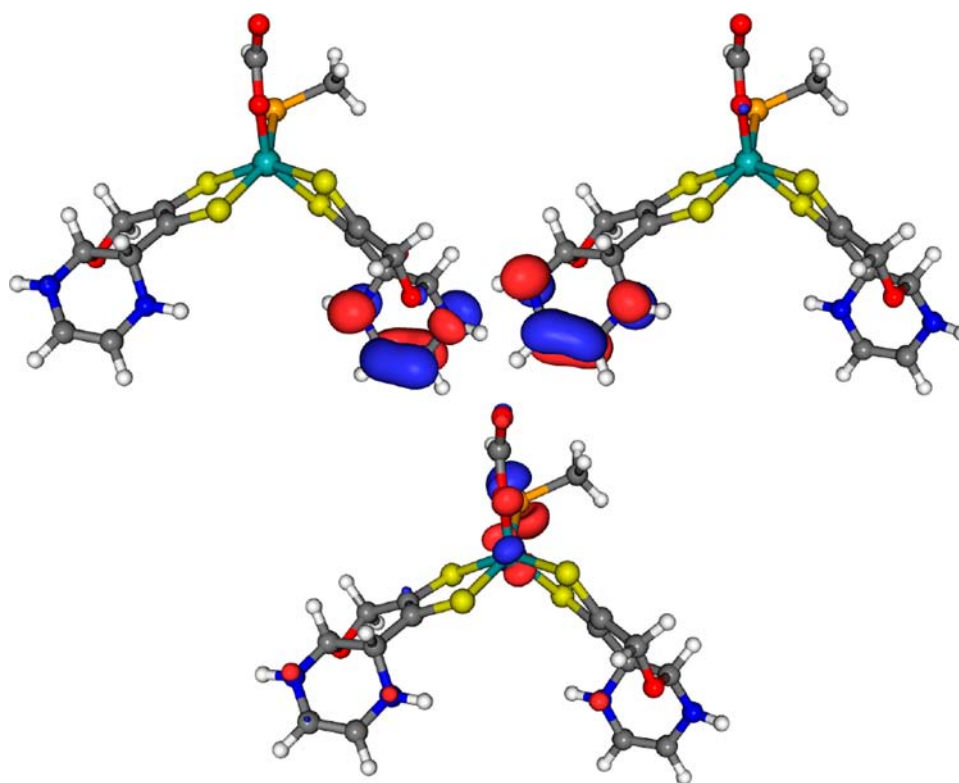


Figure 5. Top: HOMO (left) and HOMO-1 (right) MOs in the optimized geometry of the reactant state in the SeH mechanism, model A. The two orbitals are quasi-degenerate in energy because they differ by less than $0.3 \text{ kcal mol}^{-1}$. Bottom: LUMO MO in the optimized geometry of the reactant state in the SeH mechanism, model A.

interact with the corresponding R333 residue.¹² Arg also forms a hydrogen bond with an O atom of the coordinated formate (1.72 \AA).

In the $S_{\text{MGD}}\text{H}$ mechanism, the H^+ acceptors are the MGD S^- atoms. Only H^+ transfer to one of the four available S atoms has been studied for symmetry reasons. Analysis of the $S_{\text{MGD}}\text{H}-\text{A}$ pathway highlights the rotation of the formate molecule and the concomitant slight bending of the $\text{Mo}-\text{O}_{\text{formate}}-\text{C}_{\text{formate}}$ angle going from the reactant to the transition state. This structural reorganization allows the HCO_2^- H atom to come closer to the acceptor S_{MGD} atom. The $\text{C}_{\text{formate}}-\text{H}$ bond is elongated to 1.78 \AA in the transition state, while the $S_{\text{MGD}}-\text{H}$ distance is 1.46 \AA . The reaction product features a square-pyramidal geometry of the Mo center, while CO_2 moves away from the active site. As for $S_{\text{MGD}}\text{H}-\text{B}$, the proton-transfer reaction pathway is similar to that of $S_{\text{MGD}}\text{H}-\text{A}$, with $\text{C}_{\text{formate}}-\text{H}$ and $S_{\text{MGD}}-\text{H}$ distances of 1.49 and 1.95 \AA , respectively. In the products, the Se ligand, which was not coordinated to the metal ion in the reactants, binds to Mo, which attains a slightly distorted octahedral coordination geometry.

The SH reaction pathway can take place only in MB reaction models. The mechanistic and structural features of the transition state are analogous to those previously discussed for $S_{\text{MGD}}\text{H}$. The Arg side chain interacts with both formate and the selenide of Se-Cys. The transition state for H^+ transfer is characterized by a $\text{C}_{\text{formate}}-\text{H}$ distance of 1.46 \AA and a $\text{S}-\text{H}$ distance of 1.97 \AA . Also, in this case in the product, the CH_3Se^- group is coordinated to the Mo ion, forming a distorted octahedral geometry. In addition, CO_2 is displaced from the active site and the guanidinium group interacts with S_{MGD} atoms and the Se atom.

The hydride transfer from formate to molybdenum (MoH) has been investigated for both MA and MB. Notably, it turned out that this pathway features low energy barriers. H^- transfer in MoH-A occurs according to a two-step mechanism, i.e., through an intermediate (**IA**) formation, which connects the two transition states **TS1A** and **TS2A**. In **TS1A**, the Mo complex retains the overall distorted trigonal-prismatic coordination geometry encountered in reactants, while the coordinated HCO_2^- tilts over the metal ion so that the H atom gets closer to Mo (2.02 \AA) and the $\text{C}_{\text{formate}}-\text{H}$ bond is stretched from 1.12 \AA in the reactant up to 1.36 \AA . **IA** is then formed, which features the $\text{C}_{\text{formate}}-\text{H}$ bond shortening to 1.22 \AA , whereas the $\text{Mo}-\text{H}$ and $\text{Mo}-\text{O}_{\text{formate}}$ distances are almost unchanged compared to **TS1A**. In addition, **IA** shows a significant elongation of the $\text{Mo}-\text{O}$ bond compared to the reactants. **TS2A** is associated with the actual hydride transfer to Mo: the $\text{C}_{\text{formate}}-\text{H}$ distance increases to 1.62 \AA , and also the $\text{O}_{\text{formate}}-\text{Mo}$ distance increases to 2.77 \AA . Such a step can be referred to as an actual β -elimination of H, *vide infra*). The $\text{Mo}-\text{H}$ product (**I'A**) shows a distorted trigonal-prismatic coordination of the Mo center, with CO_2 leaving the active site. Finally, H^+ transfer from Mo to the coordinated Se ligand closes the $\text{H}^+/2\text{e}^-$ process. The barrier associated with this step (see **TS3A**; Figure 2) is $15.4 \text{ kcal mol}^{-1}$. The energetic profile of the entire MoH-A pathway reveals the key effect exerted by the Mo ion, which acts as a mediator of the H-transfer process.

The MoH-B pathway is quite different from the corresponding MA route. It is worth recalling that in MB the Se ligand is not originally bound to Mo. In fact, in the reactant, the Se atom is replaced by one of the formate O atoms. Nevertheless, as observed in the previous $S_{\text{MGD}}\text{H}$ and SH mechanisms, the Se coordination to Mo is restored because of the presence of a

vacant site on Mo, which opens up as the produced CO_2 detaches from the metal ion. Differing from the other two mechanisms, the MoH reaction pathway entails the formation of metal hydride as a product, thus saturating the first coordination sphere of Mo.

Several reaction pathways have been tested for the MoH-B reaction mechanism (see also Figure S2 in the Supporting Information and the text below). Remarkably, the one characterized by the lowest-energy barrier features SH deprotonation and concomitant CH_3Se^- protonation (Figure 4; $\text{R} \rightarrow \text{R}'$). Mota et al. proposed that the SH ligand could indeed be found in an unprotonated form.¹¹ Moving from R' , hydride transfer and simultaneous decarboxylation occur through **TS1B** (Figures 3 and 4) in a single step, thus differing from MoH-A.

TS1B features the decoordination of formate from Mo ($\text{O}_{\text{formate}}\text{-Mo}$: 3.88 Å), while in the reactant geometry associated with this catalytic step, the HCO_2^- O atom is still coordinated to Mo. Once again (see MoH-A description), when referring to such a peculiar reaction intermediate ($\text{R}'\text{B}$, Figure 4), the proposed mechanism can be conceived to involve β -elimination of a H atom to the metal ion and is typical of metal formates that undergo decarboxylation, forming the corresponding hydrides. Such a crucial event is also occurring during catalysis of the water–gas shift reaction.^{27,28} It is worth noting that whereas in MoH-A the term β -elimination can be used both referring to reactants and their subsequent **TS**, in MoH-B such definition can be adopted only when referring to reactants ($\text{R}'\text{B}$). After **TS1B**, a metal hydride intermediate **IB** is formed, in which the S^{2-} ligand is still unprotonated. It is worth noting that two routes alternative to the pathway shown in Figure 4 might be followed: first, H transfer from formate in **R** to Mo in **IB** might occur without the proton shift from SH to Se-Cys (see Figure 4; **TS1'B**) and, second, **IB** formation might be bypassed through a direct HCO_2^- -to- S^{2-} proton shift (see Figure S2 in the Supporting Information; **TS2'B**). However, both alternative mechanisms are energetically disfavored relative to the pathway going through **TS1B**.

The final H transfer (from Mo to S^{2-}) occurs through **TS2B** (see Figure 3 for structural details), with an activation barrier of 8.2 kcal mol⁻¹; essentially, **TS2B** is characterized by a slight stretching of the Mo–H and S–H bonds and features a smaller S–Mo–H angle relative to **IB**. The products formed after **TS2B** are the same obtained in the SeH pathway. The MoH-B route evidences the role of Mo as a favorable mediator for H transfer. In fact, such a pathway is the most viable among those investigated, featuring a global energy barrier of 14.1 kcal mol⁻¹ (corresponding to the maximum energy span associated with the reaction profile; see Figure 4, $E_{\text{TS2B}} - E_{\text{R}}$). B3LYP calculations have been subsequently performed to confirm the obtained results also by employing a different (hybrid) functional for the treatment of the electron exchange correlation. The resulting energy profiles (see Figures S3 and S4 in the Supporting Information) are in full agreement with the general outcome, which shows that metal-mediated pathways for H transfer are favored over other mechanisms.

NBO/NPA calculations have been performed (see Tables 2 and 3 for detailed numerical results) for evaluating atomic partial charges and their variations upon reaction. In most mechanisms, the Mo charge in the products decreases significantly (by 0.30–0.40 e) compared to that observed in the reactants, consistent with reduction of the Mo^{VI} ion. The total charge of formate increases by 0.44–0.60 e on going from

the coordinated HCO_2^- to CO_2 , implying that the electron density lost by formate during its oxidation is not completely recovered by the Mo ion. In fact, NPA shows the electron density coming from HCO_2^- oxidation is also spread on the pyrazine moiety of the cofactor, thus remarking the importance of a large-sized representation of the MGDs in DFT calculations.²⁶ These findings fit well also with the electron transmission mechanism proposed for FDH-H because the MGD conjugated ring system represents the minimum path for the electrons to reach the Fe_4S_4 cluster, which is found in the FDH-H X-ray crystal structure.¹⁴ Frontier orbital analysis (Figure 5) performed on the cofactor model shows that, in most cases, the LUMO involves only the Mo ion and some coordinating atoms. The HOMO (SOMO for triplet states) is mainly located on the rings of the pyranopyrazine moiety (Figure 5), confirming once again the importance of a reliable modeling of the MGD ligand.

CONCLUSION

In conclusion, DFT has been used to investigate systematically all possible intimate mechanisms associated with the rate-determining step of the $\text{HCOO}^- \rightleftharpoons \text{CO}_2 + \text{H}^+ + 2\text{e}^-$ reaction, catalyzed by the FDH. The sampling completeness of the mechanistic investigation focused on the H-transfer step is guaranteed by the limited number of possible H acceptors within the FDH active site. Actually, the acceptor range is composed by the S ligands of MGD, the selenide of the Se-Cys, and the Mo ion. An accurate model of the MGD ligand has been employed, in order to fulfill recently emerged requirements for the correct treatment of the cofactor stereoelectronic features.²⁶ Among all investigated mechanisms, those featuring an initial hydrogen migration as hydride from the substrate to the metal ion have turned out to be the lowest in energy, regardless of the model employed (MA vs MB, with the latter featuring the absolute lowest-energy barriers) for the enzyme active site. Notably, the conserved Se-Cys retains an important role because it is involved in shuttling protons from and to the metal cofactor. The proposal of the possible role played by the Mo ion as a mediator of H transfer from (to) formate to (from) the Se-Cys has been reinforced by using two different among the most popular (and generally reliable) electron density functionals, namely, the pure BP86 and the hybrid B3LYP. The observation that part of the electron density arising from HCO_2^- oxidation is localized on the pyrazine moiety of the cofactor, as well as localization of HOMO/SOMO on the same region, confirms that employing an extended model of the cofactor is mandatory for describing properly the chemistry of FDH and MPT binding enzymes in general.

Examples of high-valent molybdenum hydride complexes have already been reported.^{29–31} In particular, even though rare, thiolate-coordinated molybdenum hydrides have been spectroscopically characterized.²⁸ Moreover, group 6B carbonyl hydrides, such as $[\text{HM}(\text{CO})_5]^-$ ($\text{M} = \text{Cr}, \text{Mo}, \text{W}$), can perform $\text{HCOO}^- \rightleftharpoons \text{CO}_2 + \text{H}^+ + 2\text{e}^-$ interconversion.²⁸ In light of our results, the combination of a low-valent M center with strong acceptor ligands, as observed in $[\text{M}(\text{CO})_5]$ complexes, could be tentatively conceived as analogous to high-valent Mo ligated by electron donors, as in the FDH active site. Actually, the computed Mo partial charges in FDH models and the $[\text{HMo}(\text{CO})_5]^-$ complex are comparable (Table 2). This observation further supports the idea that hydride transfer may be a viable pathway in the FDH catalytic mechanism. Its strong resemblance with a key step of the catalytic mechanism

of a long-standing inorganic process, such as the water–gas shift reaction, is noteworthy. Concerning the CO₂ reductive process, the proposed mechanism fulfills the paradigmatic requirement of generating an activated metal hydride, which is able to perform a nucleophilic attack to the C atom.²

■ ASSOCIATED CONTENT

■ Supporting Information

Computational details. This material is available free of charge via the Internet at <http://pubs.acs.org>.

■ AUTHOR INFORMATION

Corresponding Author

*E-mail: giuseppe.zampella@unimib.it.

Author Contributions

The manuscript was written through contributions of all authors. All authors have given approval to the final version of the manuscript.

Notes

The authors declare no competing financial interest.

■ REFERENCES

- (1) Finn, C.; Schnittger, S.; Yellowlees, L. J.; Love, J. B. *Chem. Commun.* **2012**, 48, 1392.
- (2) Benson, E. E.; Kubiak, C. P.; Sathrum, A. J.; Smieja, J. M. *Chem. Soc. Rev.* **2009**, 38, 89.
- (3) Mark, T.; et al. *Chem. Rev.* **2001**, 101, 953.
- (4) Oloman, C.; Li, H. *ChemSusChem* **2008**, 1, 385.
- (5) *Pathways for utilization CO₂—opportunities and challenges, research and innovation*; Det Norske Veritas: Atlanta, GA, 2011.
- (6) Enthaler, S.; von Langermann, J.; Schmidt, T. *Energy Environ. Sci.* **2010**, 3, 1207.
- (7) Reda, T.; Plugge, C. M.; Abram, N. J.; Hirst, J. *Proc. Natl. Acad. Sci. U.S.A.* **2008**, 105, 10654.
- (8) Leonhartsberger, S.; Korsia, I.; Bock, A. *J. Mol. Microbiol. Biotechnol.* **2002**, 4, 269.
- (9) Moura, J. J. G.; Brondino, C. D.; Trincao, J.; Romao, M. J. *J. Biol. Inorg. Chem.* **2004**, 9, 791.
- (10) Romao, M. J. *Dalton Trans.* **2009**, 4053.
- (11) Mota, C. S.; Rivas, M. G.; Brondino, C. D.; Moura, I.; Moura, J. J.; Gonzalez, P. J.; Cerqueira, N. M. J. *J. Biol. Inorg. Chem.* **2011**, 16, 1255.
- (12) Raaijmakers, H. C. A.; Romao, M. J. *J. Biol. Inorg. Chem.* **2006**, 11, 849.
- (13) Leopoldini, M.; Chiodo, S. G.; Toscano, M.; Russo, N. *Chem.—Eur. J.* **2008**, 14, 8674.
- (14) Boyington, J. C.; Gladyshev, V. N.; Khangulov, S. V.; Stadtman, T. C.; Sun, P. D. *Science* **1997**, 275, 1305.
- (15) Khangulov, S. V.; Gladyshev, V. N.; Dismukes, G. C.; Stadtman, T. C. *Biochemistry* **1998**, 37, 3518.
- (16) Schäfer, A.; Huber, C.; Ahlrichs, R. *J. Chem. Phys.* **1994**, 100, 5829.
- (17) Becke, A. D. *Phys. Rev. A* **1988**, 38, 3098.
- (18) Perdew, J. P. *Phys. Rev. B: Condens. Matter* **1986**, 33, 8822.
- (19) Andrae, D.; Haeussermann, U.; Dolg, M.; Stoll, H.; Preuss, H. *Theor. Chim. Acta* **1990**, 77, 123.
- (20) Galan, F.; Fouassier, M.; Tranquille, M.; Mascetti, J.; Pàpai, I. *J. Phys. Chem. A* **1997**, 101, 2626.
- (21) Mascetti, J.; Galan, F.; Pàpai, I. *Coord. Chem. Rev.* **1999**, 190–192, 557.
- (22) Schafer, A.; Klamt, A.; Sattel, D.; Lohrenz, J. C. W.; Eckert, F. *Phys. Chem. Chem. Phys.* **2000**, 2, 2187.
- (23) Ahlrichs, R.; Bar, M.; Haser, M.; Horn, H.; Kolmel, C. *Chem. Phys. Lett.* **1989**, 162, 165.
- (24) Reed, A. E.; Weinhold, F. *J. Chem. Phys.* **1983**, 78, 4066.

- (25) (a) Becke, A. D. *J. Chem. Phys.* **1992**, 96, 2155. (b) Becke, A. D. *J. Chem. Phys.* **1993**, 93, 5648. (c) Stevens, P. J.; Devlin, F. J.; Chabrowski, C. F.; Frisch, M. J. *J. Chem. Phys.* **1994**, 98, 11623. (d) Lee, C.; Yang, W.; Parr, R. G. *Phys. Rev.* **1988**, B37, 785.
- (26) (a) Ryde, U.; Schulzke, C.; Starke, K. *J. Biol. Inorg. Chem.* **2009**, 14, 1053. (b) Matz, K. G.; Mtei, R. P.; Rothstein, R.; Kirk, M. L.; Nieter Burgmayer, S. *J. Inorg. Chem.* **2011**, 50 (20), 9804.
- (27) Eisenberg, R.; Hendriksen, D. E. *Adv. Catal.* **1979**, 28, 79.
- (28) (a) Darensbourg, D. J.; Fischer, M. B.; Schmidt, R. E., Jr.; Baldwin, B. J. *J. Am. Chem. Soc.* **1981**, 103, 1297. (b) Darensbourg, D. J.; Rokicki, A.; Darensbourg, M. Y. *J. Am. Chem. Soc.* **1981**, 103, 3223.
- (29) Burrow, T. E.; Hills, A.; Hughes, D. L.; Lane, J. D.; Lazarowych, N. J.; Maguire, M. J.; Morris, R. H.; Richards, R. L. *J. Chem. Soc., Chem. Commun.* **1990**, 1757.
- (30) Albinati, A.; Togni, A.; Venanzi, L. M. *Organometallics* **1986**, 5, 1785.
- (31) Cimadevilla, F.; Garcia, M. E.; Garcia-Vivo, D.; Ruiz, M. A.; Rueda, M. T.; Halut, S. *J. Organomet. Chem.* **2012**, 699, 67.